Supporting Information

In-situ synthesized copper-incorporated laser-induced graphene enabling high-sensitivity flexible temperature sensing

Zhihuan Wang,[a] Pei Ding,*[abc] Xuan Jia,[a] Jiahao Xu,[a] Zhicheng Luo,[a] Mingyu Li, [ab] and Dongxia Chen, [ab]

[a] School of Materials Science and Engineering, Zhengzhou University of Aeronautics, Zhengzhou, China

[b] Henan Key Laboratory of Aeronautical Materials and Applied Technologies, Zhengzhou University of Aeronautics, Zhengzhou, China

[c] Collaborative Innovation Center of Processing and Detecting for Aerospace High Performance Materials, Henan Province, China

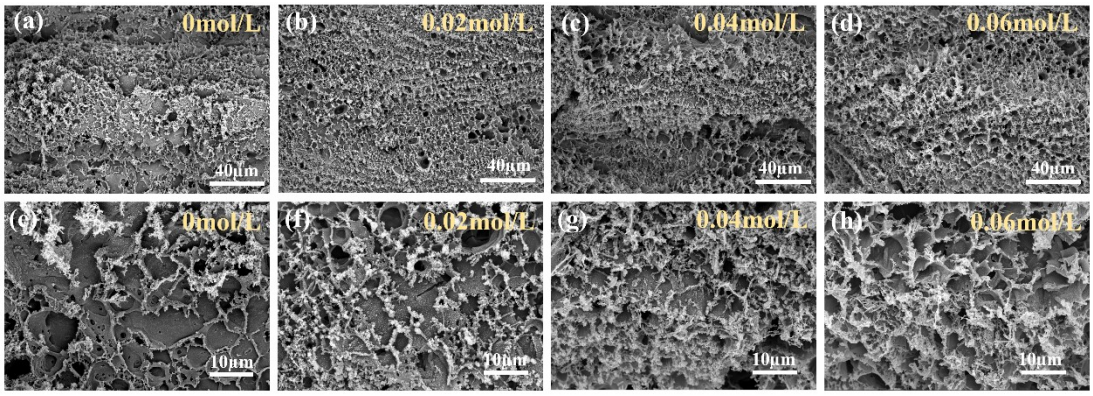

Fig. S1 SEM images of the Cu@LIG series samples prepared at different $CuCl_2$ concentrations. The laser power is uniformly set at 4W during the preparation process.

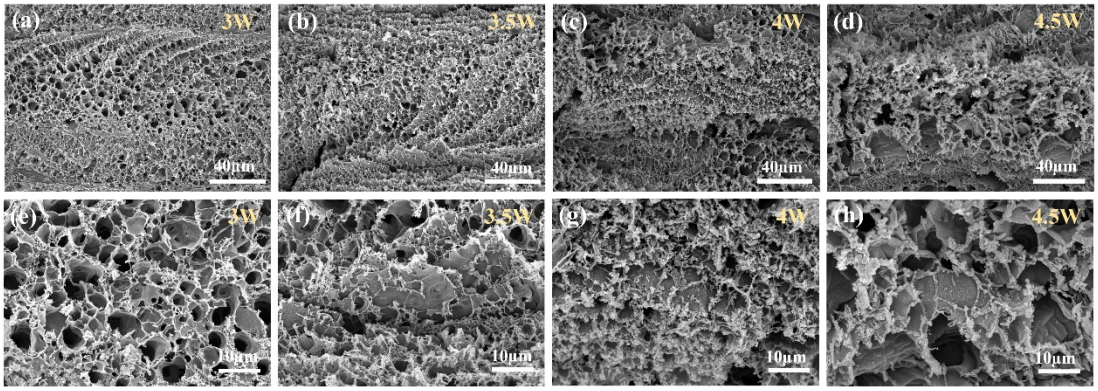

Fig. S2 SEM images of the Cu@LIG series samples prepared under different laser powers. The concentration of $CuCl_2$ in the precursor is fixed at 0.04 mol/mL.

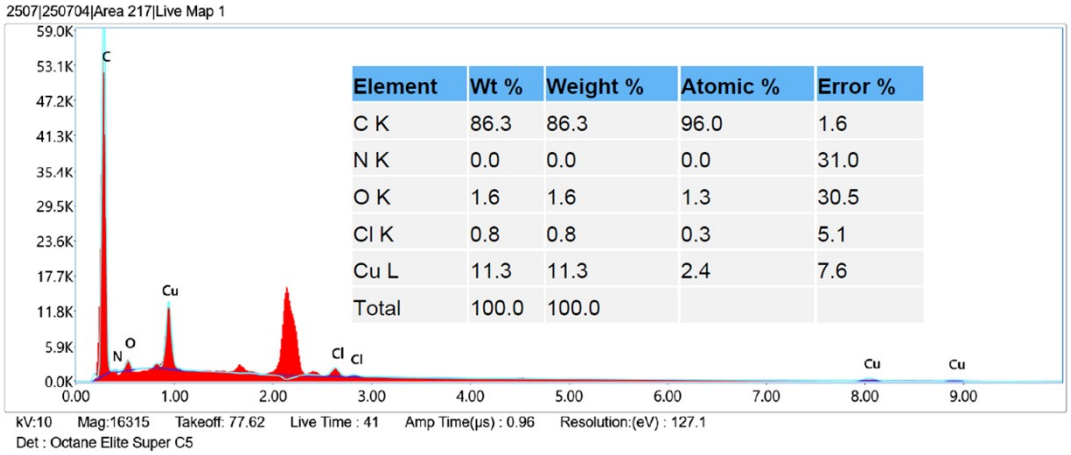

Element	Wt %	Weight %	Atomic %	Error %
C K	86.3	86.3	96.0	1.6
N K	0.0	0.0	0.0	31.0
O K	1.6	1.6	1.3	30.5
Cl K	0.8	0.8	0.3	5.1
Cu L	11.3	11.3	2.4	7.6
Total	100.0	100.0		

Fig. S3 EDS analysis of the Cu(0.04)@LIG(4) sample during the SEM test.

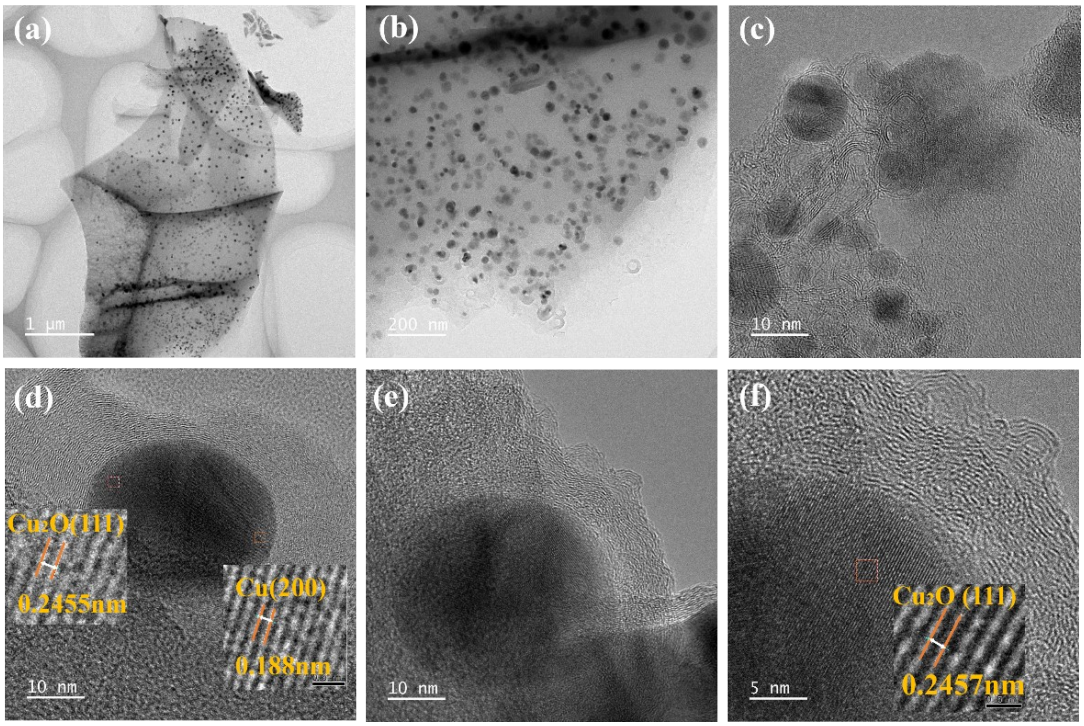

Fig. S4 TEM images of Cu(0.04)@LIG(4) sample.

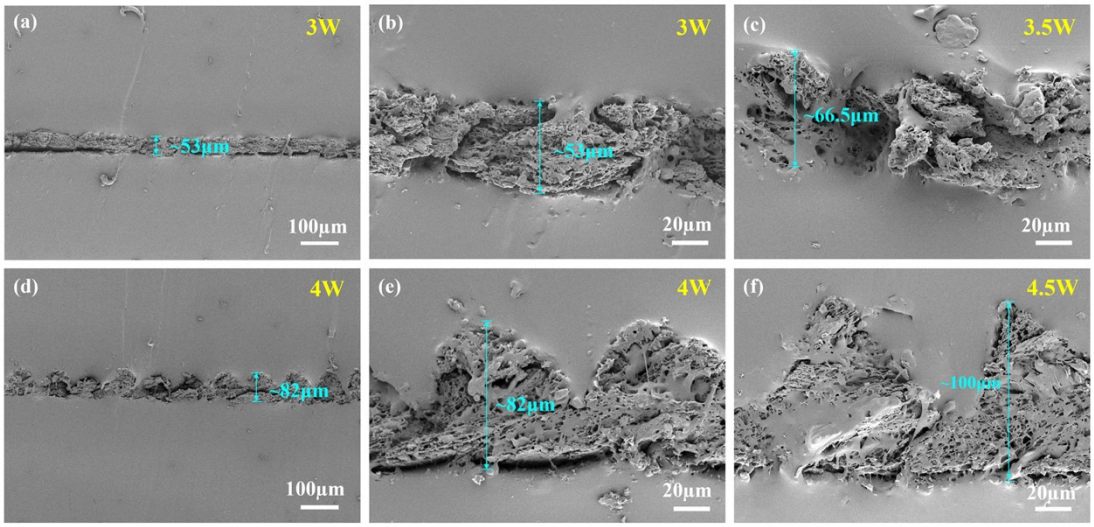

Fig. S5 SEM images of PDMS/Cu(0.04)@LIG/PDMS series samples prepared under different laser power.

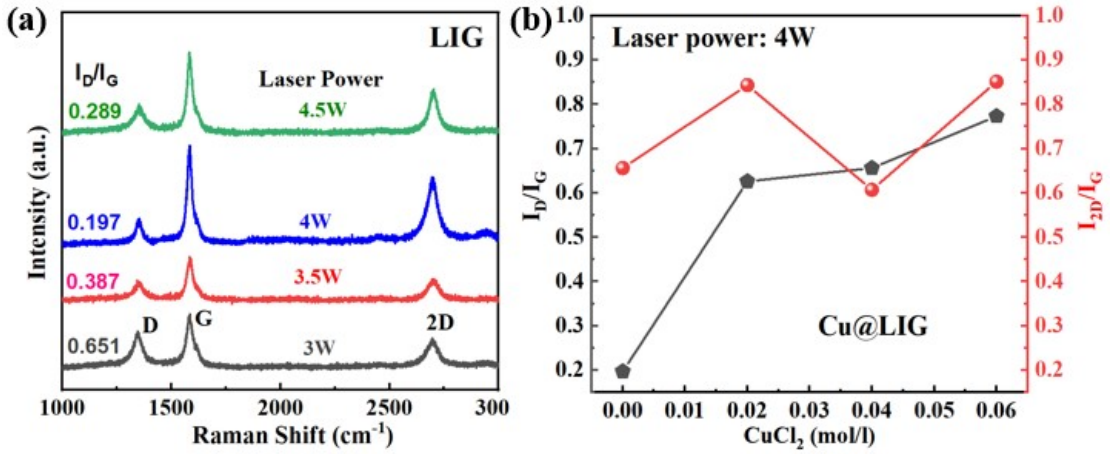

Fig. S6 (a) Raman spectra of LIG prepared under different laser power. (b) D/G and 2D/G peak intensity ratio of Cu@LIG samples prepared at the same laser power (4 W) but different $CuCl_2$ doping concentration.

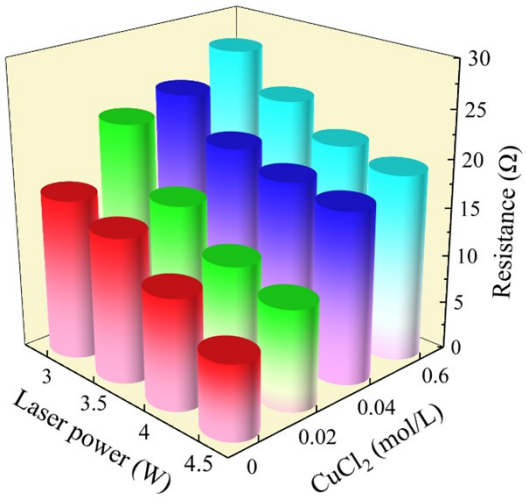

Fig. S7 Effect of laser power during the preparation process and the concentration of $CuCl_2$ in the precursor on the resistance of the resulting Cu@LIG.

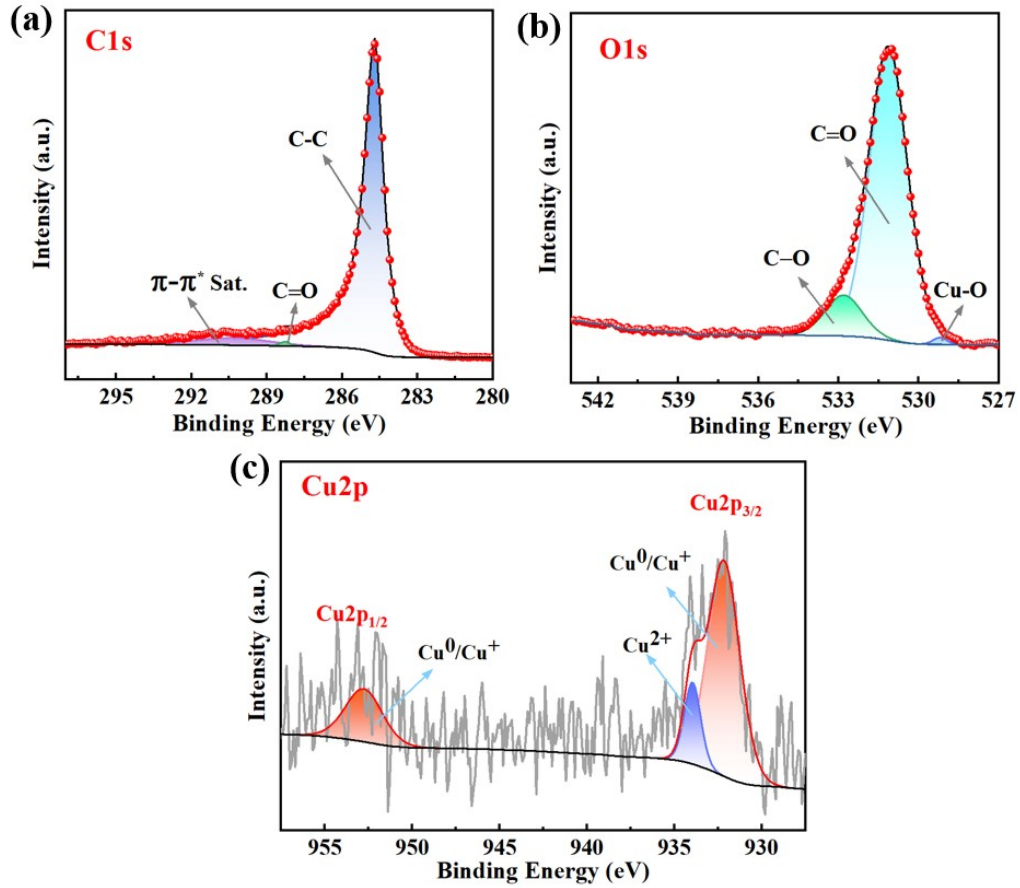

Fig. S8 XPS analysis of Cu(0.04)@LIG(4)/PI sample. (a)-(b) High-resolution C 1s and O 1s spectra obtained from the sample surface. (c) High-resolution Cu 2p spectrum collected from the cross-section through micro-area XPS (spot size: 30 μm).

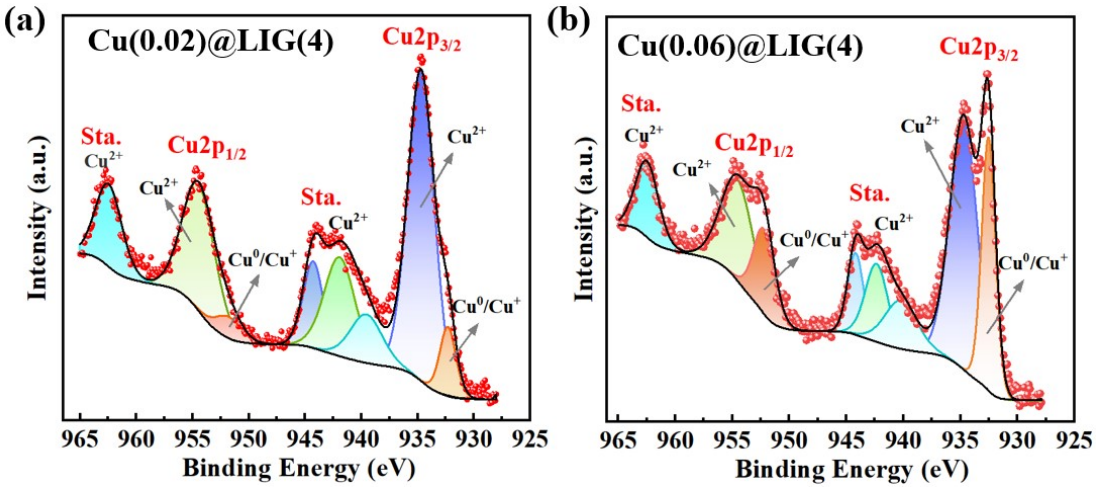

Fig. S9 High-resolution Cu 2p spectra of the Cu(0.02)@LIG(4)/PI and Cu(0.06)@LIG(4)/PI surfaces.

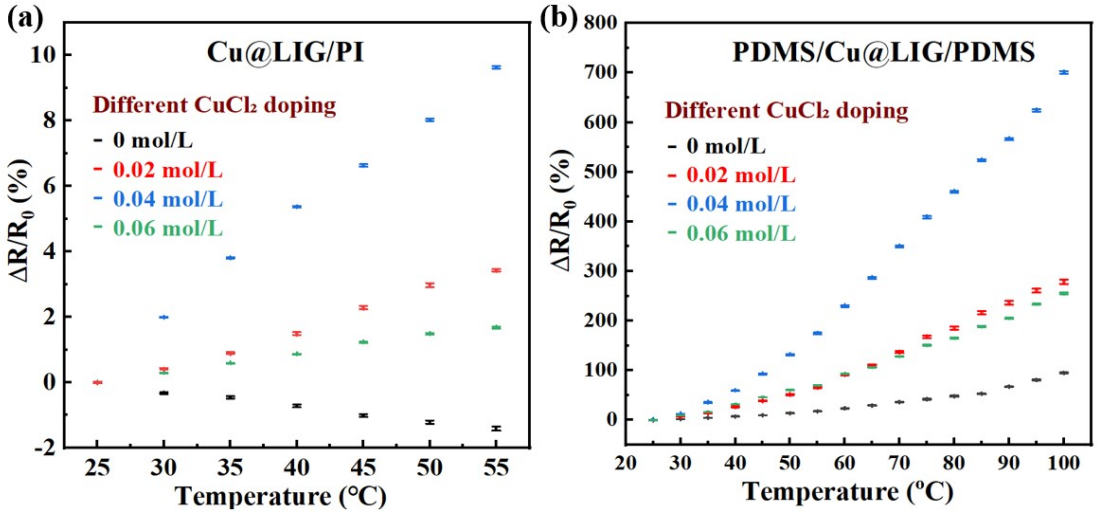

Fig. S10 Temperature-dependent relative resistance change ($\Delta R/R_0$) of the Cu@LIG/PI and PDMS/Cu@LIG/PDMS series samples. The mean values with standard deviation error bars ($n \geq 3$) are ploted.

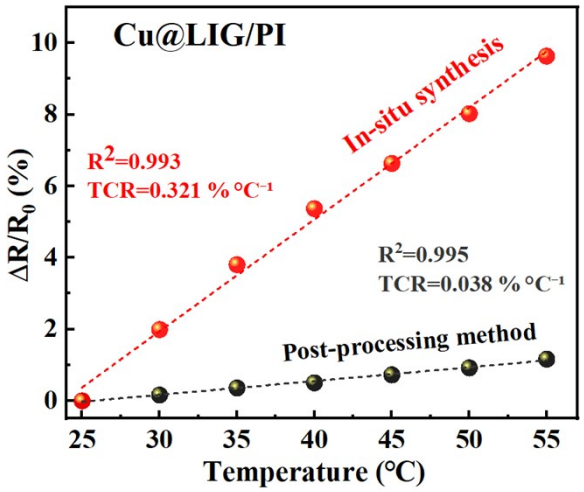

Fig. S11 Relative resistance changes of the Cu(0.04)@LIG(4)/PI samples prepared by laser in-situ synthesis and post-processing methods. The post-treated sample was obtained by first spray-coating a 0.04 mol/L $CuCl_2$ solution onto the LIG/PI substrate, followed by secondary laser irradiation (4 W).

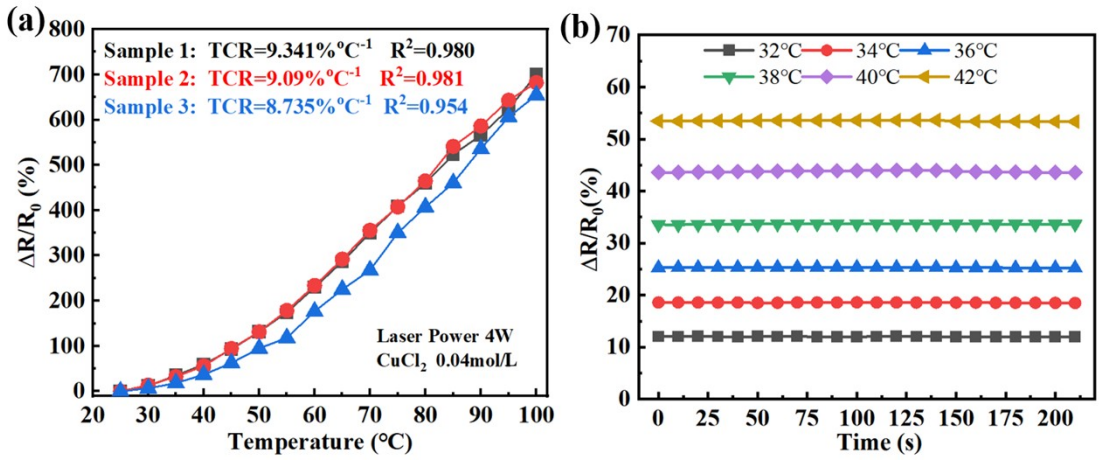

Fig. S12 (a) Temperature-dependent resistance change curves for PDMS/Cu(0.04)@LIG(4)/PDMS samples from different batches. (b) Resistance change response curve of the fabricated sensor at different temperatures.

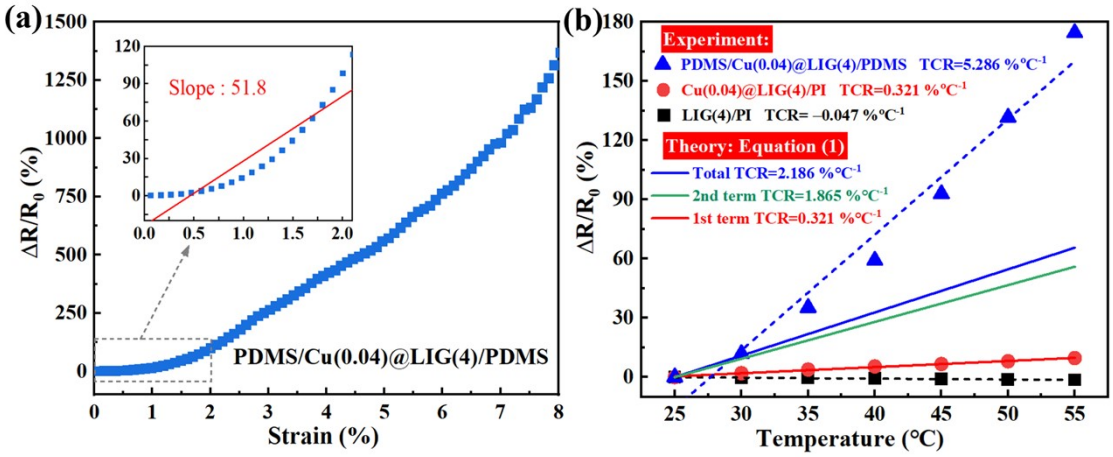

Fig. S13 (a) Measured relative resistance change as a function of strain for a PDMS/Cu(0.04)@LIG(4)/PDMS membrane. The strain gauge factor is obtained by linear fitting the measurement data within the 0–2% strain range of the sample, as shown in the inset figure. (b) Temperature-dependent relative resistivity measured in LIG(4)/PI, Cu(0.04)@LIG(4)/PI and PDMS/Cu(0.04)@LIG(4)/PDMS materials (symbols marked with different colors). Taking PDMS/Cu(0.04)@LIG(4)/PDMS as an example, the figure also illustrates the contributions of the first term, second term, and their sum (represented by lines of different colors) to the resistivity variation, derived from equation (1) based on the theoretical model.

Table S1 Comparison of the sensitivity of carbon-based flexible temperature sensors.

Sensing Materials	Substrate/Matrix	Temperature Range (℃)	TCR（%/℃）	Linearity	Reference
LIG	PI	30-100	-0.05	0.999	1
LIG	PDMS	20-100	0.25	0.98	2
LIG	Silicone	25-43	-0.3	0.999	3
LIG/LTrGO	PI	0-50	0.526	-	4
LIG/VO_x	Pluronic F127-resol	30-110	0.045	0.969	5
NiO/LIG	PI	30-100	-0.079	0.999	6
CuNPs@LIG	PVDF	30-45	-1.74	-	7
GF	PDMS	30-100	5.203	0.996	8
CB	TPU	25-60 60-100	-1.18 -0.36	-	9
N/rGO	PI	20-50	0.842	0.991	10
AgNPs/CNTs	PVA/PBGA	20-40	2.99	0.998	11
NiO/CNTF	PDMS	-15-25 25-60	-9.1 -2.1	-	12
PrGO/Cu	PI	30-40	-2.058	0.994	13
PPS/CNT	PDMS	-30-90	-0.4	0.996	14
Gr/PVDF/PANI	PDMS/PEG	20-45	-0.832	0.98	15
MXenex	PU/PVA	0-30	-5.27	-	16
Cu@LIG	PDMS	30-80 25-100 55-100	-1.11 9.341 11.38	0.98 0.999	This Work

References

1. Y. Zhang, C. Zhao, C. Yu, Y. Li, X. Guo, Y. Zhang, C. Chen and L. Cao, High-linearity graphene-based temperature sensor fabricated by laser writing. *Journal of Materials Science: Materials in Electronics*, 2024, **35**, 109.
2. J. Guo, X. Liu, Z. Sun, X. Zheng, H.-K. Sung, Z. Yao, Y. Li and Y. Li, An intelligent dual-sensing e-skin system for pressure and temperature detection using laser-induced graphene and polydimethylsiloxane. *Materials & Design*, 2024, **238**, 112640.

3. S. Duan, B. Wang, Y. Lin, Y. Li, D. Zhu, J. Wu, J. Xia, W. Lei and B. Wang, Waterproof mechanically robust multifunctional conformal sensors for underwater interactive human–machine interfaces. *Advanced Intelligent Systems*, 2021, **3**, 2100056.
4. J. Xia, W. Huang, K. Majer-Baranyi, M. Zhang and X. Zhang, Conformal temperature/impedance sensing patch based on graphene materials for nondestructive detection of fish freshness. *ACS Applied Materials & Interfaces*, 2023, **15**, 45095-45105.
5. L. Yang, J. Yan, C. Meng, A. Dutta, X. Chen, Y. Xue, G. Niu, Y. Wang, S. Du, P. Zhou, C. Zhang, S. Guo and H. Cheng, Vanadium Oxide-Doped Laser-Induced Graphene Multi-Parameter Sensor to Decouple Soil Nitrogen Loss and Temperature. *Advanced Materials*, 2023, **35**, 2210322.
6. S. Wang, C. Tan, Q. Zong, A. Sett, H. Ye and P. French, In NiO-Doped Laser-Induced Graphene: A High-Performance Flexible Temperature Sensor, 2024 IEEE SENSORS. IEEE, 2024: 01-04.
7. M. Nankali, M. Soleimani, P. Enrique and P. Peng, Direct laser synthesis, tuning, and patterning of metal nanoparticles-decorated graphene for flexible temperature sensors. *Materials Today Nano*, 2025, **30**, 100617.
8. L. Chen, X. Yao, X. Liu, Z. Luo, C. Ye, C. Huang, C. Wang, C. Cai, L. Lyu and X. Wu, High throughput in–situ temperature sensor array with high sensitivity and excellent linearity for wireless body temperature monitoring. *Small Structures*, 2022, **3**, 2200080.
9. Y. He, H. Wang, W. Cao, J. Wang, L. Sun, H. Lin, K. Rui, Y. Yan and J. Zhu, Tailoring 3D conductive networks as wearable sensors for pressure or temperature sensing. *Composites Communications*, 2024, **49**, 101985.
10. J. Min, S. Huo, J. Zhu, X. Wang, Z. Xiao, W. Kong and L. Chen, Modulating carrier mobility of N-doped rGO for flexible linear temperature sensors. *Applied Materials Today*, 2025, **42**, 102584.
11. X. Yu, W. Qin, X. Li, Y. Wang, C. Gu, J. Chen and S. Yin, Highly sensitive, weatherability strain and temperature sensors based on AgNPs@ CNT composite polyvinyl hydrogel. *Journal of Materials Chemistry A*, 2022, **10**, 15000-15011.
12. Y. Lu, H. Zhang, Y. Zhao, H. Liu, Z. Nie, F. Xu, J. Zhu and W. Huang, Robust fiber-shaped flexible temperature sensors for safety monitoring with ultrahigh sensitivity. *Advanced Materials*, 2024, **36**, 2310613.
13. Y. Shin, Y. W. Kim, H. J. Kang, J. H. Lee, J. E. Byun, J.-Y. Yang and J. W. Lee, Stretchable and skin-mountable temperature sensor array using reduction-controlled graphene oxide for dermatological thermography. *Nano Letters*, 2023, **23**, 5391-5398.
14. Y. Zhang, J. Jin, Y. Zhang, D. Mei and Y. Wang, Flexible Temperature Sensor with Wide Sensing Range and Fast Response Enabled by PEDOT:PSS/CNT and Thermal Management Encapsulation. *ACS Applied Electronic Materials*, 2025, **7**, 5981-5993.
15. C. Zhang, W. Wei, Y. Li, X. Li, Y. Liu, X. Wang and S. Chen, Sweat and Deformation-Resistance Graphite/PVDF/PANI-Based Temperature Sensor for Real-Time Body Temperature Monitoring. *Advanced Materials Technologies*, 2024, **9**, 2400149.
16. H. Liu, C. Du, L. Liao, H. Zhang, H. Zhou, W. Zhou, T. Ren, Z. Sun, Y. Lu and Z. Nie, Approaching intrinsic dynamics of MXenes hybrid hydrogel for 3D printed multimodal intelligent devices with ultrahigh superelasticity and temperature sensitivity. *Nature Communications*, 2022, **13**, 3420.